Two modes of interfacial pattern formation by atmospheric pressure helium plasma jet-ITO interactions under positive and negative polarity

2017 J. Phys. D: Appl. Phys. 50 195203

(http://iopscience.iop.org/0022-3727/50/19/195203)

IOP Publishing Journal of Physics D: Applied Physics

J. Phys. D: Appl. Phys. **50** (2017) 195203 (10pp) https://doi.org/10.1088/1361-6463/aa6915

Two modes of interfacial pattern formation by atmospheric pressure helium plasma jet-ITO interactions under positive and negative polarity

Zhijie Liu[1], Dingxin Liu[1,4], Dehui Xu[1], Haifeng Cai[1], Wenjie Xia[1], Bingchuan Wang[1], Qiaosong Li[1] and Michael G Kong[1,2,3,4]

[1] State Key Laboratory of Electrical Insulation and Power Equipment, Centre for Plasma Biomedicine, Xi'an Jiaotong University, Xi'an City 710049, People's Republic of China
[2] Frank Reidy Center for Bioelectrics, Old Dominion University, Norfolk, VA 23508, United States of America
[3] Department of Electrical and Computer Engineering, Old Dominion University, Norfolk, VA 23529, United States of America

E-mail: liudingxin@mail.xjtu.edu.cn and mglin5g@gmail.com

Received 22 January 2017, revised 19 March 2017
Accepted for publication 24 March 2017
Published 18 April 2017

Abstract

In this paper, we report the observation of an interfacial pattern formation on the ITO surface by atmospheric pressure helium plasma jet-ITO interactions. By changing the voltage polarity of positive and negative pulses, the interfacial phenomenon displays two different pattern modes, i.e. a double ring pattern with a combination of homogeneous and filamentous modes as well as a single ring pattern with a homogeneous mode. The reasons may mainly be attributed to the spread of a radially outward traveling surface ionization wave that would cause electric field distributions and charge accumulations on the ITO surface. The spatial-temporal distribution of $N_2^+(B^2\sum_u^+)$, He($3s^3S$), and O($3p^5P$) emissions are diagnosed to better understand the formation mechanism and the differences of plasma jet patterns under positive and negative polarities. Results show that the distribution of $N_2^+(B^2\sum_u^+)$ emission is the main contributor for generating the filament structure in a double ring pattern for positive polarity, the homogeneous mode pattern mainly depends on the distribution of O($3p^5P$) emission for positive and negative polarity. Additionally, in order to further systematically understand the behaviors of plasma jet patterns, some parametric results, such as behaviors versus pulse peak voltage, dielectric material, pulse repetition rate, and flow rate are investigated. Some interesting phenomena and additional insights for the plasma jet pattern are found with different parametric conditions. This study might help to better understand effects of plasma jets in interaction with surfaces, or its application in the medical sector.

Keywords: surface ionization wave, atmospheric pressure plasma jet, reactive species, pulse polarity, spatial-temporal distribution

(Some figures may appear in colour only in the online journal)

[4] Author to whom any correspondence should be addressed.

1. Introduction

In the last few years, atmospheric pressure plasma jets (APPJs) have attracted considerable interest as a source of chemically and biologically active species for applications in material processing and biological medicine [1–3]. In many cases, the treated surface or workpiece by discharge plasma is a dielectric material that can retain surface charge, for example, organic materials in industrial processing or living tissue (or *in vitro* cultures) in new medical therapies. Thus a proper understanding of the mechanisms of delivery of reactive species to dielectric surfaces and the nature of charge accumulation and electric field distribution are vital for optimizing APPJs to suit a particular application [4–6].

Up to now, there have been many experimental and computational research that focused on investigating the free plasma jet under different parameter conditions, in which helium (He) plasma jet flows into ambient air without interruption, i.e. without consideration of the plasma–surface interaction [5–9]. This physical mechanism regarding free plasma jets propagating in open air is well understood. However, the knowledge of plasma–surface interactions is in severe deprivation [10, 11]. In applications of APPJs treating a surface, for instance a polymer in industrial processing or living tissue in new medical therapies, the interaction becomes quite complicated because it would not only deform the electric field distribution on contact, but also affects the fluxes of significant particles delivered to the dielectric surface [10–12]. Recently, a number of computational studies have simulated the behavior of plasma jets interacting with dielectric materials [10, 11, 13–17], such as Breden *et al* who investigated the roles of distance from the gas exit tube to the target, target thickness, and dielectric properties on APPJ-surface interactions excited by nanosecond pulse voltages; the results were found to be that the fluxes of radical and ionic species at the dielectric surface decreases with increasing dielectric thickness, and that the gas gap distance significantly affects the fluxes of reactive species delivered to the surface [13]. Norberg *et al* presented a computational study of an APPJ impinging on materials with varying permittivity. They confirmed that the electrical properties of the surface, the production of charged and reactive species on the surface, and the discharge dynamics of the plasma jet are all significantly affected by changing the relative permittivity of the material being treated [14]. Even if the computational study of APPJ impinging on the dielectric surface has been conducted and some theoretical knowledge has been understood in a certain extent, the mechanism research of interaction between APPJs and dielectric surface, especially in experimental studies, are not yet fully understood [10, 17]. The mechanism associated with the interaction of APPJs with dielectric surfaces is of significant practical interest. In particular, it is important to understand the nature of the discharge dynamics of the APPJ impinging on a dielectric surface [13], the distribution of active species in space and time, and the reasons for different modes of plasma jet–surface interaction. Such works would hold a far-reaching significance in the surface modification and biological sterilization [1, 4].

In this paper, we present two kinds of modes of pattern by a He APPJ-ITO interaction;specifically, how the evolution of the pattern of APPJ-ITO interaction observed though the spatial-temporal distribution of $N_2^+(B)$, He($3s^3S$), and O($3p^5P$) emissions is affected by each others interactions controlled by positive and negative polarities. In addition, some experimental behaviors under several key parameter conditions are performed, such as pulse peak voltage, pulse repetition rate, dielectric material, and flow rate to analysis the dynamic behavior of the plasma jet interacting with dielectric materials.

2. Experimental setup

Figure 1 shows a schematic illustration of the experimental setup of APPJ, the generator is made up of two parts, one is a T-shape cylindrical quartz tube, the other is a stainless steel needle with a length of 10 cm and a diameter of 0.1 mm, which is located in the center of quartz tube (od.: 6 mm, id.: 4 mm) and fixed in place by a rubber plug. The side of the needle with a length of 3 cm is located outside of tube, and the other side of the needle is 15 mm away from the nozzle of tube. The quartz tube is wrapped with a copper sheet with a length of 10 mm, which is located 10 mm from the open end of tube. An ITO glass plate with a thickness of 1 mm is perpendicular to the center axis of the quartz tube and is located 10 mm from the nozzle of tube. The side of insulating layer of ITO is facing toward the tube nozzle. The purity of He gas, as a working gas, is supplied into the tube from a gas inlet at a flow rate of 5 slm. A homemade nanosecond pulse generator with a rising time of about 40 ns and pulse duration of 1 μs is used to generate the plasma jet. The electrical characteristics are measured by a digital oscilloscope equipped with voltage/current probes (P6015A and P6021, Tektronix) and the optical emission spectroscopy (OES) is detected by an Andor SR-750i grating monochromator (grating grooving 1200 lines mm^{-1}). The instantaneous images of self-organized patterns with an exposure time of 5 ns are obtained by an ICCD camera (PI-MAX3, Princeton Instruments) equipped with different waveform optical filters. Note that in figure 1(a), the needle electrode is connected to the pulse generator as both the powered electrode and copper sheet are connected to the grounded electrode; this case is called positive polarity, on the contrary, it is called negative polarity in figure 1(b). The image of patterns of He APPJ-ITO interaction captured by a digital camera with an exposure time of 1000 ms at 9.6 kV pulse peak voltage, 4 kHz pulse repetition rate, and 5 slm flow rate are displayed in figures 1(c) and (d) under positive and negative pulse polarity. Upon interaction with ITO glass under positive polarity, it can be observed that the plasma spreads out across the surface and generates streamerlike ionization fingers that branch out and propagate across the surface; this finally generates the plasma jet pattern with a double ring structure in figure 1(c), e.g. the inner ring pattern is the homogeneous mode and the outer ring pattern

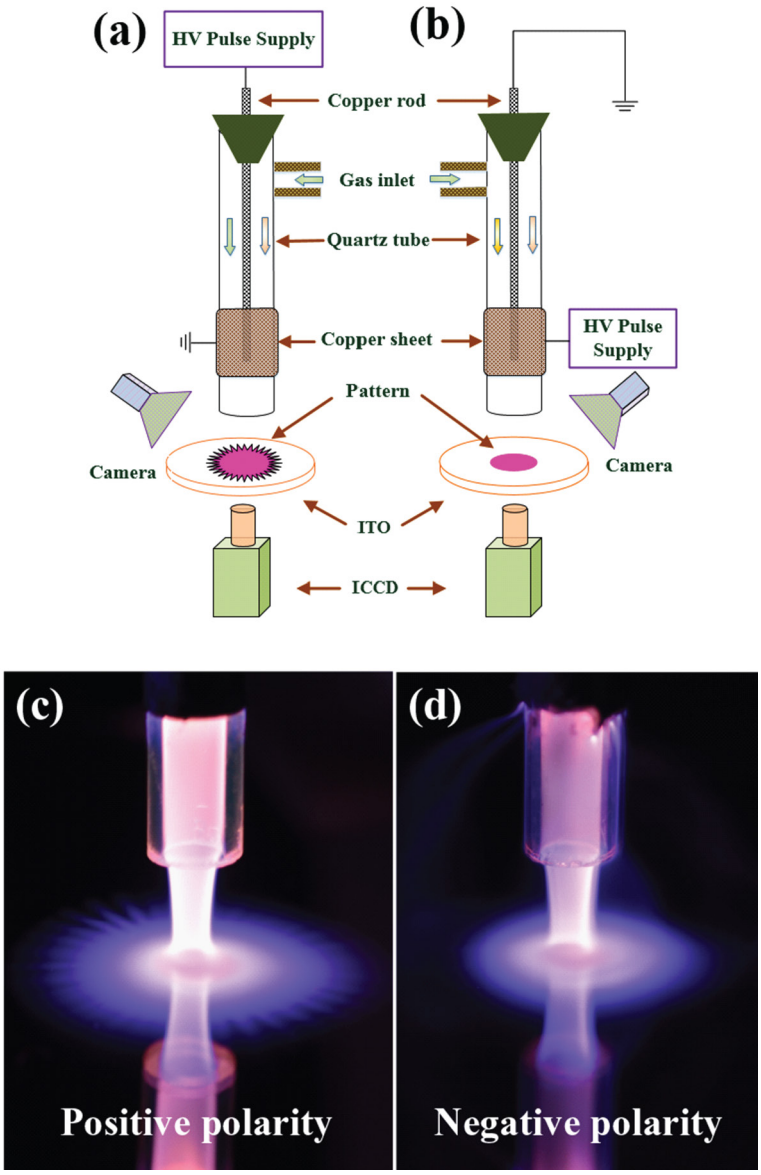

Figure 1. (a) and (b) Schematic illustration of the experimental setup of plasma jet-ITO interaction, (c) and (d) the plasma jet patterns under positive and negative polarity.

is the filament mode, these two modes are separated by a clear dividing line. With respect to the negative polarity, it is found that the plasma spreads along the radial direction and forms a homogeneous pattern with a single ring structure (figure 1(d)), and the pattern has a relatively smaller area. These two different pattern modes indicate two kinds of interaction mechanisms and distribution of active species on the surface. Due to the reflective effect of ITO glass, the inverted reflection of plasma jet can also be observed in images. The waveforms of pulse voltage and current of the plasma jet for positive and negative pulses are shown in figure 2 with 9.6 kV and 4 kHz. Note that the plasma jet is only produced during the rise-edge and fall-edge phases, as evidenced by the current peaks. Meanwhile, the pulse current peak for positive polarity can reach up to 250 mA at the rising-edge period, while the value is only 150 mA for negative polarity, this difference may be attributed to the different space electric fields formed between the propagating ionization fronts and the charges accumulation.

3. Results and discussion

3.1. The spatial-temporal behavior of the pattern of APPJ-ITO interaction

In order to investigate the spatial-temporal behavior of the pattern of APPJ-ITO interaction, the time-resolved images of patterns produced by APPJs-ITO interaction for positive and negative polarities are taken by the ICCD camera and shown in figure 3. The time range from 10 ns to 1250 ns chosen from a single pulse cycle (in figure 2) is utilized to analyse the microscopic evolution of the pattern of APPJ-ITO interaction in figure 1. As for the ICCD images under positive polarity, in the initial phase form 10 ns to 600 ns, plasma

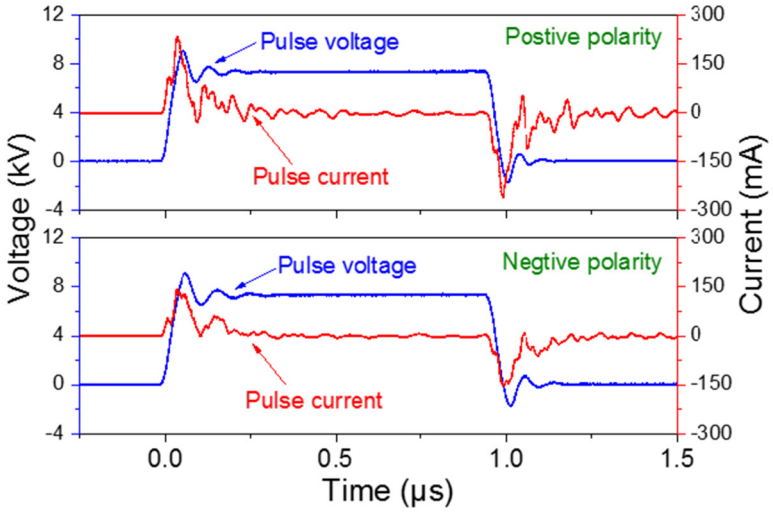

Figure 2. The waveforms of pulse voltage and current of plasma jets under positive and negative polarity.

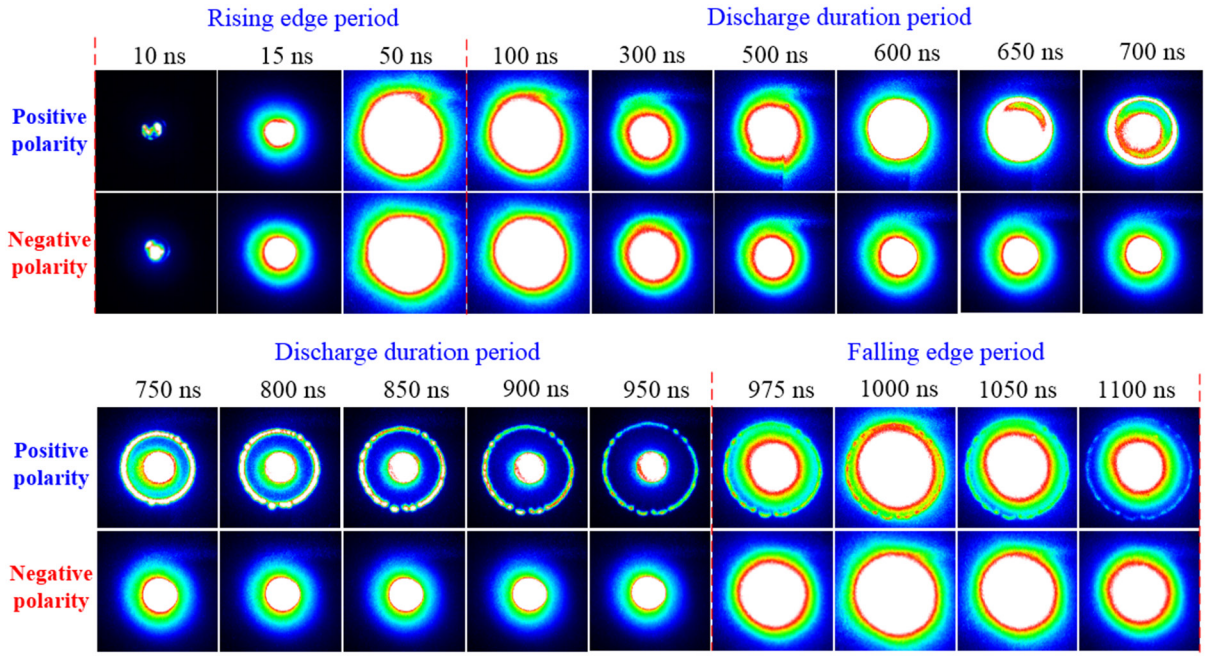

Figure 3. The ICCD images of plasma patterns produced by APPJs-ITO interaction under positive and negative polarity.

bullets start from the initial breakdown within the dielectric tube and propagates into open air. At about 600 ns, the fast ionization wave eventually reaches the dielectric surface and then gradually spreads along the radial direction on the surface to form the double ring structure at 750 ns. As time goes on, the outer ring still continues to spread and begins to fracture into many small segments at 800 ns, which are regarded as the main reason to generate the filaments of plasma jet pattern in figure 1(c). The falling edge period of pulse voltage takes place at 975 ns, the area of plasma jet pattern suddenly increases and reaches its largest size at 1000 ns, where it also obtains its strongest intensity. Finally, the intensity of the plasma jet pattern gradually weakens and the area of the plasma jet pattern decreases. As for the ICCD images under negative polarity, it is clearly found that the plasma jet pattern always keeps the single ring structure with a homogeneous mode no matter the discharge duration period or falling edge period. The similar evolution behaviors also take place compared to that of positive pulse at falling edge periods while the homogeneity of plasma jet patterns is unchanged under negative polarity.

3.2. The measurement of optical emission spectroscopy

To identify reactive species from plasma jet patterns under positive and negative polarity, the OES in the wavelength range from 300 nm to 800 nm is shown in figure 4, via the head of optical fibers placed vertically to the center of the pattern. From figure 4, it can be found that the emission spectra is mainly dominated by $N_2^+(B)$, He($3s^3S$), and O($3p^5P$) emissions; additionally, the emission line of OH($A^2\Sigma$), $N_2(C^3\Pi_u)$, H_α and H_β can also be detected. Reactive species such as $N_2^+(B)$, O($3p^5P$), OH($A^2\Sigma$), and $N_2(C^3\Pi_u)$ produced are not only attributed to high energy electron excitation, but also energy transfer from

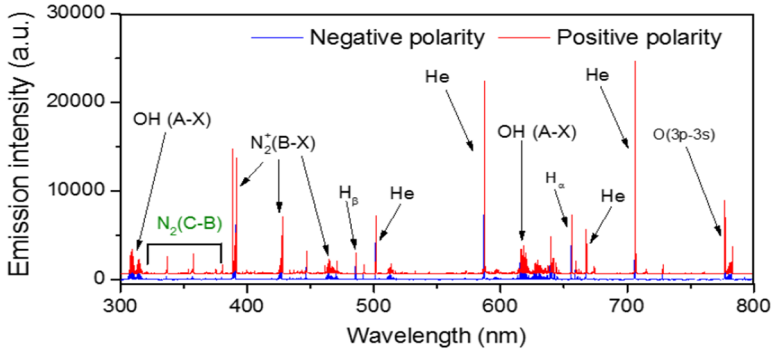

Figure 4. The OES from the plasma jet patterns, (a) positive polarity, and (b) negative polarity.

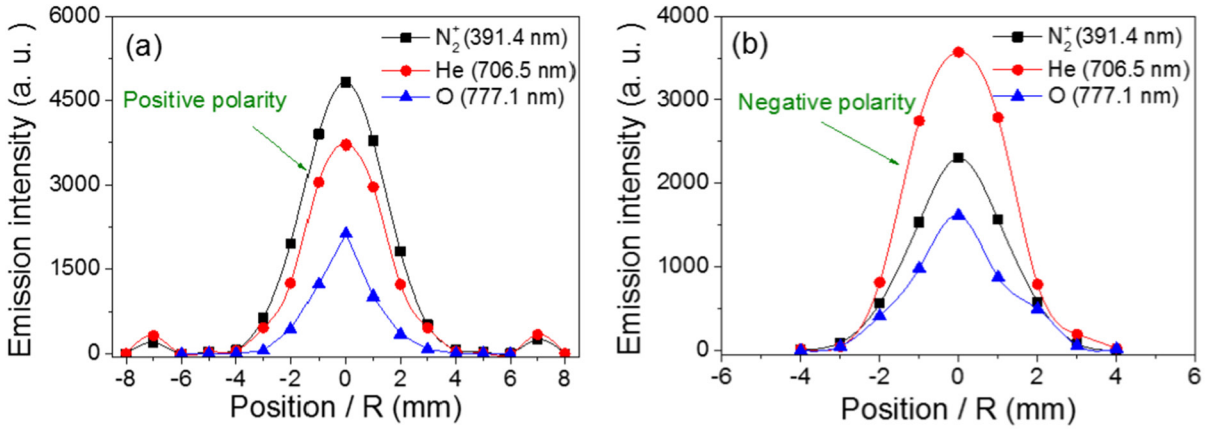

Figure 5. Spatially distribution of the $N_2^+(B)$, He($3s^3S$), and O($3p^5P$) for plasma jet patterns along the radial direction under positive (a) and negative (b) polarity.

He metastable state [18, 19]. It is also found that the intensity of $N_2^+(B)$, He($3s^3S$), and O($3p^5P$) emissions for plasma jet patterns under positive polarity is much higher than under negative polarity; this indicates that a higher concentration of reactive species can be produced in the plasma pattern of positive polarity.

To clarify the uniformity and the spatial distribution feature of reactive species on the plasma jet patterns, the spatially resolved OES of excited state $N_2^+(B)$, He($3s^3S$), and O($3p^5P$) are examined along the radial direction under positive and negative polarity, with the results shown in figures 5(a) and (b), respectively. It is found that the $N_2^+(B)$, He($3s^3S$), and O($3p^5P$) display a near-symmetrical distribution of emission profiles, the distribution is relatively uniform in the middle part and then decreases gradually toward both ends, and finally approaches zero. The $N_2^+(B)$ and He($3s^3S$) emissions display the greatest intensity at the center of the distribution profile, and the O($3p^5P$) emission displays the weakest . The difference between figures 5(a) and (b) is that the emission profile area of positive polarity is wider between −8 mm and 8 mm in the radial direction, while the emission profile area of negative polarity is thinner and only range from −4 mm to 4 mm; this also confirms that the former pattern for positive pulse has a larger dimension. Additionally, two small peaks at the two edges of plasma jet pattern in figure 5(a) can be observed, which is attributed to some filament channels with high current formed, although the fast ionization waves become weaker at this position.

For a small energy gap between rotational levels, the equilibrium between translational motion and rotational motion is readily achieved because of frequent collisions among heavy particles at atmospheric pressure, thus, the gas temperature of the plasma is approximately equal to the rotational temperature (T_{rot}) [20]. To determine the T_{rot} of the plasma jet pattern, the emission spectra of the OH($A^2\Sigma \rightarrow X^2\Pi$, 0–0) band and $N_2^+(B^2\sum_u^+ \rightarrow X^2\sum_g^+$, 0–0) are used to calculate the rotational temperature by comparing experimental and simulation spectra using the LIFBASE software [21]. The best fitting simulation spectra to the experimental spectra of OH ($A^2\Sigma$) and $N_2^+(B)$ bands are shown in figure 6, at 9.6 kV pulse peak voltage and 4 KHz pulse repetition rate. The T_{rot} is estimated at 365 ± 10 K for OH($A^2\Sigma$) and at 350 ± 10 K for N_2^+ (B). To study the plasma gas temperature distribution on the surface of ITO, the gas temperature varies as a function of the radial direction of circular patterns under positive and negative polarity (figure 7). As shown in figure 7, it is clearly found that the plasma gas temperature also display a near-symmetrical distribution, the maximum value of gas temperature is shown in the center of the plasma jet pattern, and then gradually decreases toward to both ends. However, the gas temperature under positive polarity is higher than under negative polarity.

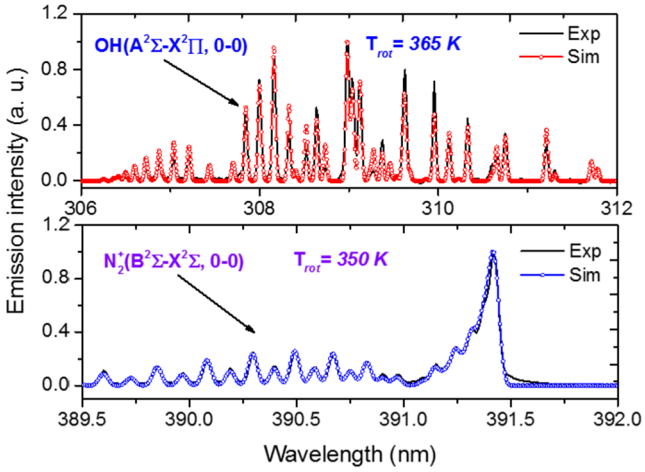

Figure 6. Plot of the experimental and simulation spectra for patterns at 9.6 kV pulse peak voltage and 4 KHz pulse repetition rate.

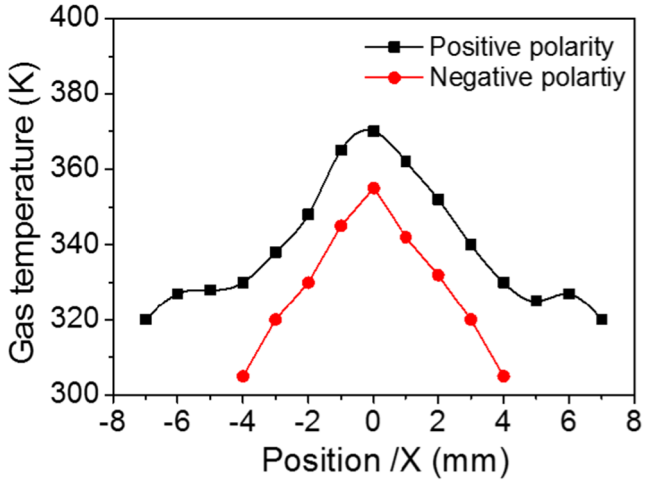

Figure 7. The plasma gas temperature varies as a function of the radial direction of patterns under positive and negative polarity.

3.3. The evolution of spatial-temporal distribution

So far, some urgent questions about two modes plasma patterns have been proposed: firstly, how active species distribute on the pattern in real time? Secondly, which active species are responding when producing filament mode of pattern? Thirdly, which active species are the main contributors for generating a uniform plasma pattern? It would be satisfying to solve these questions if the spatial-temporal distribution of simplex reactive species from plasma patterns can be accurately detected using an ICCD camera with optical filter of different spectra ranges; because the separated studies of species may offer us a better way to understand the evolution of plasma jet patterns in real time. Since the active species of $N_2^+(B)$, He($3s^3S$), and O($3p^5P$) are main constituents of the full-spectra emission, they are chosen to study the evolution of the spatial-temporal distribution for plasma jet patterns. As shown in figure 8(a), under positive pulse, the reactive species of $N_2^+(B)$, He($3s^3S$), and O($3p^5P$) exhibit three different kinds of spatial-temporal distribution behaviors. For $N_2^+(B)$, the double ring structure also happens and gradually spreads along the radial direction; the emission of $N_2^+(B^2\sum_u^+)$ is mainly concentrated in the center and outer ring. More interesting is that the outer ring also presents a fractured phenomenon and shows similar temporal change behaviors compared to that of all species distribution on plasma jet patterns with the increase of evolution time, it is confirmed that $N_2^+(B)$ is regarded as the main contributor for generating the filament structure of the outer ring of patterns. As for the He($3s^3S$), the He($3s^3S$) emission also displays a double ring structure at 600 ns, which pulls ahead at least 100 ns compared to the $N_2^+(B)$ emission, this difference is attributed to their different spreading speeds and lifetime resulting in the time out of synchronous when the fast ionization wave reaches the surface of the ITO glass. As for the O($3p^5P$) distribution, the O($3p^5P$) emission has a homogeneous distribution in the whole plasma jet pattern region. At the falling aged period, both the intensity and plasma jet pattern distributions rise abruptly and then fade away, but the distribution of O($3p^5P$) can be maintained for a long time on the ITO surface. From figure 8(b), it is found that the spatial-temporal distribution of $N_2^+(B)$, He($3s^3S$), and O($3p^5P$) always show a homogeneous single ring structure, which is an extremely similar change behavior compared to the distribution of all reactive species of plasma jet patterns, which is also the most different compared to the evolution behavior in figure 8(a). Furthermore, the distribution of O($3p^5P$) is more homogeneous and gentler on the surface of ITO glass compared to the distribution of $N_2^+(B)$ and He($3s^3S$) no matter the plasma jet pattern produced under positive and negative pulse polarity. Therefore, it is reasonably concluded that the distribution of O($3p^5P$) emission is the main contributor for generating the homogeneous mode of plasma jet pattern. These attributes may enable a more accurate interpretation of how gas plasmas interact with the biological environment, and potentially allows for the deconvolution of the direct action of whole plasma from reactions with primary and secondary plasma species [1].

Based on the above experimental results, it is clearly found that the properties of plasma jets excited by positive and negative polarity are quite different, which results in the different change behaviors and pattern modes when the bullet head reaches the surface of ITO glass. These two obvious phenomena are attributed to different propagating mechanisms of ionization wave on the surface under positive and negative polarity. As for positive polarity, when the plasma jet is ignited, the electrons with high energy quickly move toward to the needle electrode and generate many reactive species, of which the positive ions that accumulated at the front of the plasma jet bullet would effectively enhance the applied electric field. Corresponding higher concentrations of excited species is generated due to the higher electric field and higher speed of ionization rate. The plasma jet bullet including many excited species under the action of electric field force is accelerated to propagate and collide with glass surface to form plasma jet patterns [22, 23]. As reported in the literature published by Wang *et al* [11], who confirmed that O_2^+ and $N_2^+(B)$ are distributed along the streamer body, the maximum density of $N_2^+(B)$ is located in the streamer head, and

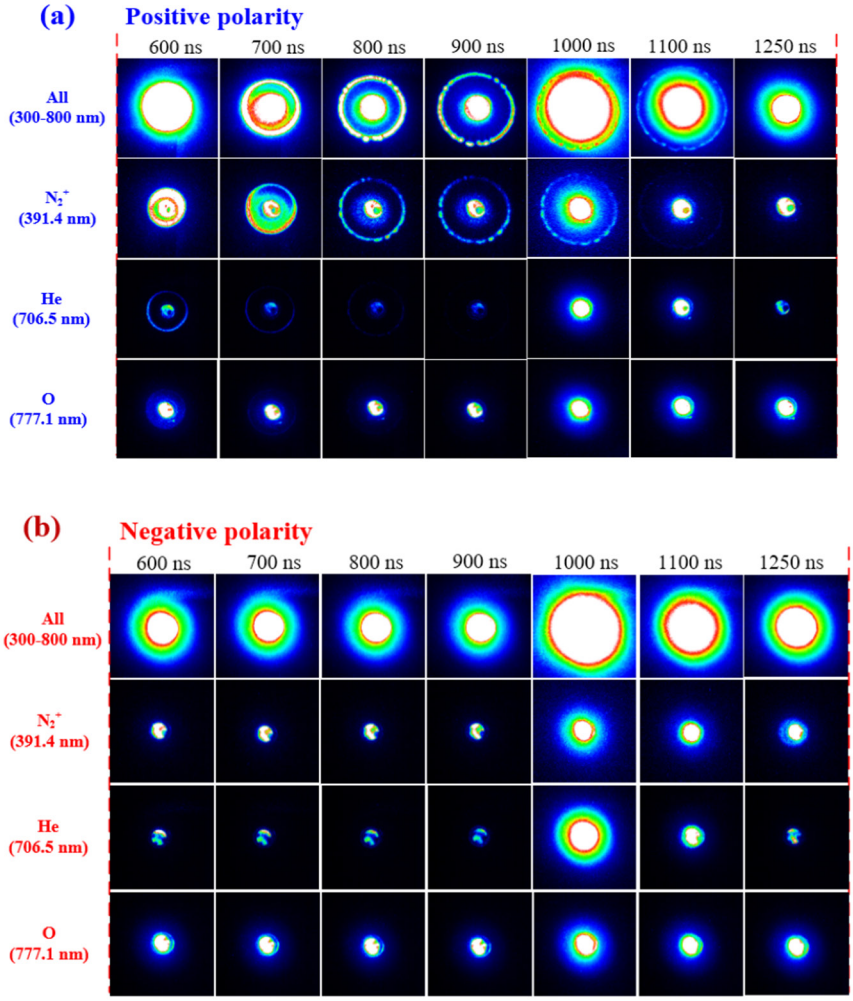

Figure 8. Spatial distribution of $N_2^+(B)$, He($3s^3S$), and O($3p^5P$) for plasma jet patterns along the radial direction under positive (a) and negative (b) polarity.

has the highest density of positive ions at the dielectric surface, the penning ionization is the major ionization reaction along the streamer body as well as in the streamer head. As for the negative polarity, the electrons from needle electrodes have a lower velocity to move toward the space and recombine with positive ions, such as $N_2^+(B)$, which leads to the reduction of the quantity of positive ions and weakens the applied electric field in the discharge region [24]. So the plasma jet bullet with lower concentrations of excited species is obtained and collides with the glass surface to produce single pattern of negative pulse.

The homogeneous and filament modes of plasma jet patterns would be explained by the perspective of the spread of a radially outward traveling surface ionization wave (SIW) on the ITO surface. Before the plasma jet bullet reaches the ITO surface, the He plasma jet occupies a dominant status in the plasma column into the tube, when the bullet propagates into open air, small amounts of air diffuses into the He plume and will produce bright emissions from O_2 and N_2. For this reason, all reactive species are bright in the center. As the SIW starts to spread along the radial direction when the plasma jet bullet reaches the ITO surface, more and more air is diffuses into the He plume that is dispersed along the surface. So the weaker SIW (compared to the central He plasma plume) dominantly excites the N_2 to form $N_2^+(B)$ in the radially expanding of SIW, since the weaker SIW would not provide enough energy to result in forming a filamentous structure of the outer ring of plasma jet pattern under positive polarity. The He emission in SIW in figure 8(a) is very early when the reduced electric field E/N (where E is the electric field and the N is the particle number density) in the SIW is higher, the E/N in the SIW decreases as SIW expands, which results in the He emission and metastable He^* weakening and disappearing. There is little O emission because most of the O is produced by either dissociative attachment or dissociative excitation transfer from metastable He^* in the radially expanding SIW, and there is not much He^* produced by the weaker SIW. This spreading of an SIW has been predicted computationally by several researchers. For example, papers by Kushner's group [4, 9, 14, 16, 17].

3.4. The behaviors of pattern under different parameter conditions

In order to further systematically understand the behaviors of plasma jet patterns, some parametric results, such as behavior versus pulse peak voltage, dielectric material, pulse repetition

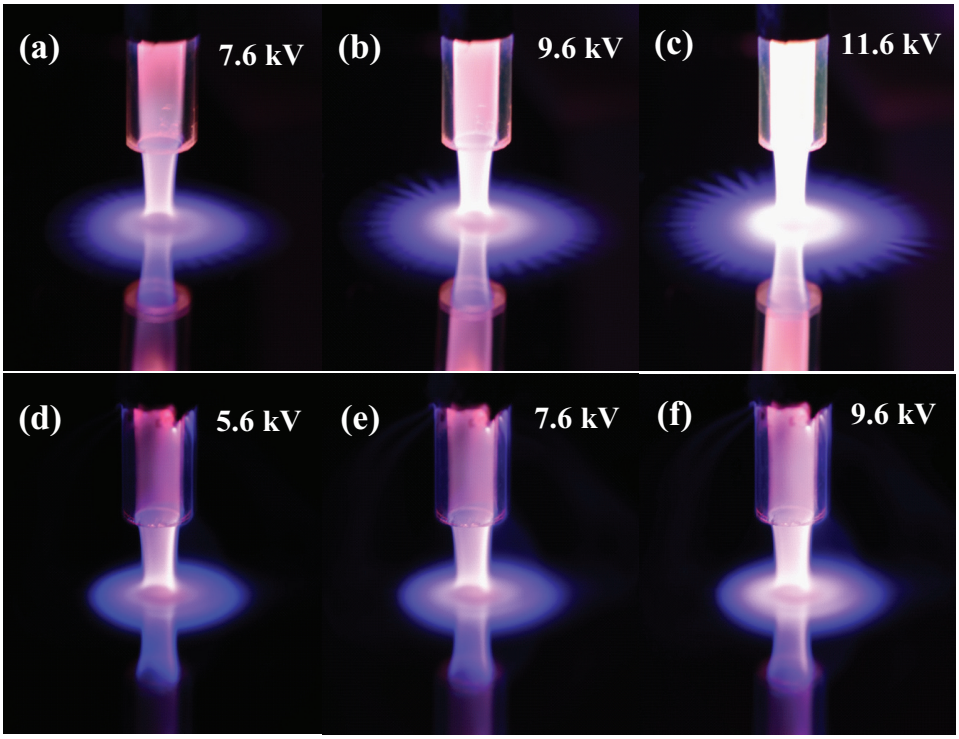

Figure 9. The images of plasma jet pattern under positive polarity (a)–(c) and negative polarity (d)–(f) with different pulse voltages.

rate, and flow rate, are shown in below experiments; which not only provides systematic trends, but also provides some interesting phenomena and additional insights. Figure 9 shows the images of plasma jet patterns with the variation of pulse voltages at 4 kHz pulse repetition rate under positive and negative polarity. It can be seen that the plasma jet pattern under positive polarity presents a double ring structure with homogeneous and filamentous modes. With the increase of pulse voltage, the filamentous structure on the pattern becomes more and more obvious and the area of the plasma jet pattern gradually extends on the ITO surface. However, as for the plasma jet pattern under negative polarity, the pattern always presents a single ring structure with homogeneous mode and the area of plasma jet pattern increases slowly when the pulse voltage is increased from 5.6 kV to 9.6 kV. Increasing the pulse peak voltage would cause higher SIW and *E*/*N* on the material surface, therefore, more production of reactive species such as metastable He*, He, O, and N_2^+ (B) in the radially expanding of SIW can be obtained.

As an important factor which can affect the homogeneity of plasma jet patterns, the effect of dielectric materials (such as ITO, quartz glass, ceramic, and PTFE) on the behaviors of plasma jet patterns excited by positive and negative polarity is shown in figure 10, the pulse peak voltage and pulse repetition rate are set to 9.6 kV and 4 kHz, respectively. With respect to the pattern under positive polarity, the plasma jet pattern interaction with dielectric materials present different pattern structures when the quartz glass, ceramic, and PTFE are used as dielectric materials that plasma jets interact with. In addition, there are a large number of filamentous that appear randomly on the outer edge of the pattern, which is in accordance with the results reported in [25]. However, for the plasma jet pattern under negative polarity, the pattern always shows a uniform pattern without any discharge filaments observed when the quartz glass, ceramic, and PTFE are used as the dielectric materials. By changing only the dielectric materials (namely changing relative permittivity) upon which a plasma jet is touched, the significant effects on the behavior of electric filed and deposited change density are realized. As reported in literature published by Kushner *et al* [14] who proposed that a lower permittivity enables greater spread of the plasma along the surface by propagation of the surface ionization wave, and allows more penetration of the electric field into the material. Results presented in above experiments might help us to understand effects of plasma jets interacting with surfaces, or its application in the medical sector [26].

Additionally, the effects of pulse repetition rate and flow rate on the behaviors of plasma jet patterns excited by positive polarity are also studied and shown in figures 11 and 12, respectively. The pulse peak voltage and flow rate in figure 11 are set to 9.6 kV and 5 slm, respectively, and the pulse peak voltage and pulse repetition rate in figure 12 are set to 9.6 kV and 4 kHz, respectively. It can be found that the pattern area of plasma jets touching ITO is obviously enlarged in the radial direction and the emission intensity of plasma jet patterns is also obviously enhanced in the whole pattern region with an increase of pulse repetition and flow rates. Because an increased pulse repetition rate and flow rate results in the plasma jet further contacting with the surface of dielectric materials, finally, the charge deposition and the electric field on the surface would increase, and the corresponding spread of propagation of the SIW along the surface would be greatly enhanced.

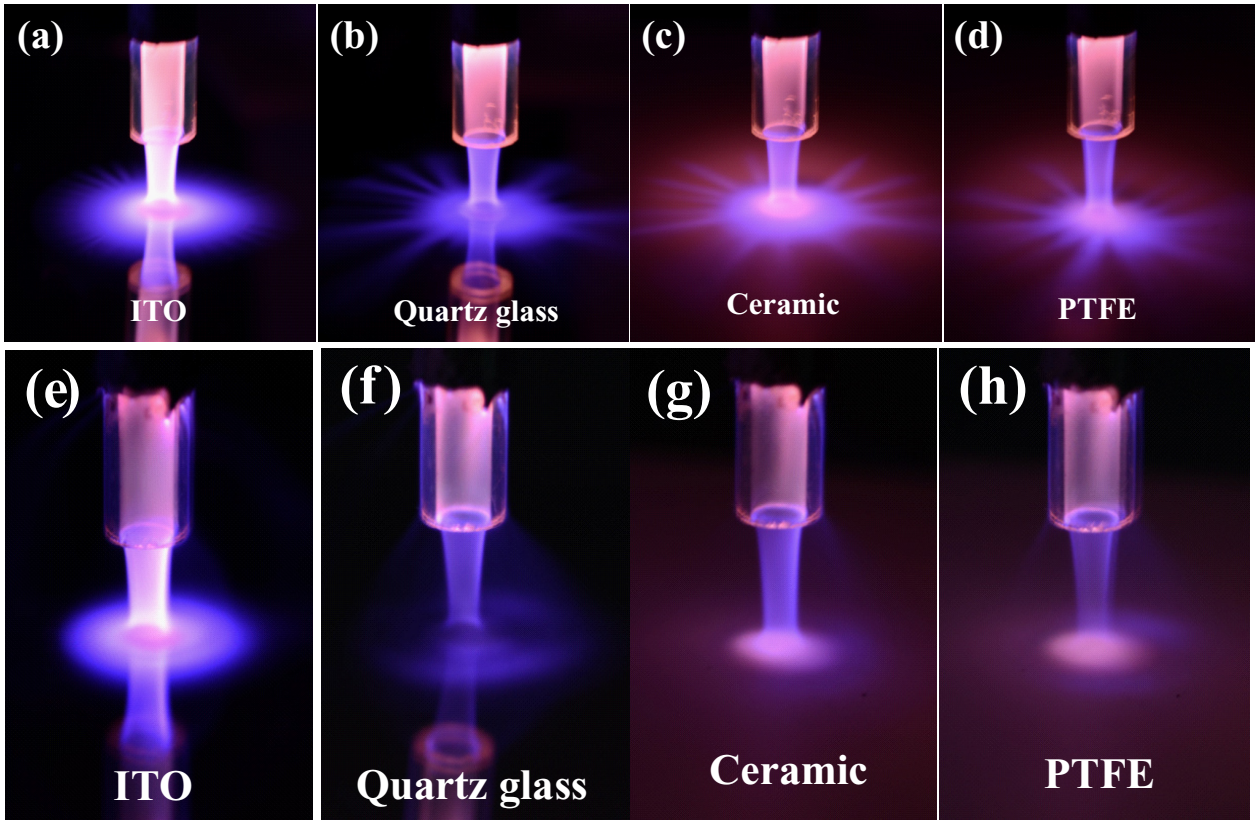

Figure 10. The images of plasma jet patterns under positive (a)–(d) and negative polarity (e)–(h) with different dielectric materials.

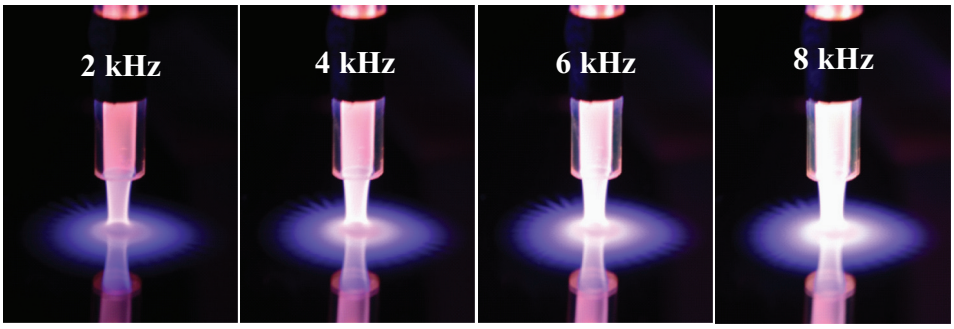

Figure 11. The effect of pulse repetition rate on the behavior of plasma jet patterns excited by positive polarity.

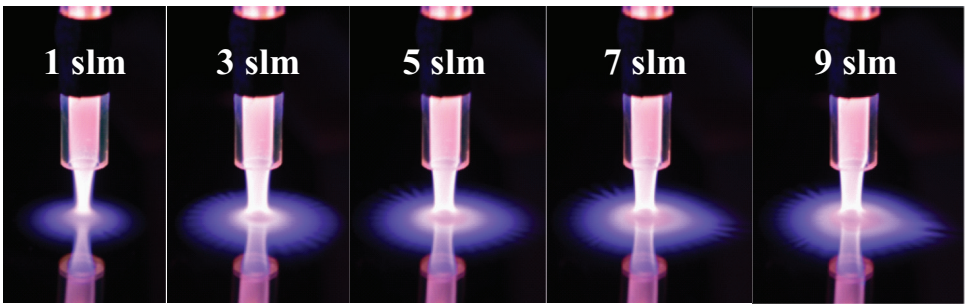

Figure 12. The effect of flow rate on the behavior of plasma jet patterns excited by positive polarity.

4. Conclusion

In conclusion, we investigated two types of different pattern mode formation by atmospheric pressure helium plasma jet-ITO interactions through changing pulse voltage polarity. These two types of different pattern modes are the double ring pattern with combination of homogeneous and filamentous modes and the single ring pattern with homogeneous mode, respectively, which may be due to the fact that the change of pulse voltage polarity causes different propagation behavior of surface ionization waves that radially spread outward that would result in different electric field distributions and charge

accumulation on the ITO surface. The spatial-temporal distribution of $N_2^+(B)$, He($3s^3S$), and O($3p^5P$) emissions exhibit quite different temporal change behaviors for plasma jet patterns under positive and negative polarity. The distribution of $N_2^+(B)$ emission is the main contributor for generating the filament structure in a double ring pattern for positive pulses, while the homogeneous mode pattern is mainly attributed to the distribution of O($3p^5P$) emission for positive and negative pulses. Additionally, the behaviors of plasma jet patterns with different parametric conditions, such as pulse peak voltage, dielectric material, pulse repetition rate, and flow rate, are investigated and discussed. It is found that the plasma jet pattern under positive polarity always presents a double ring structure with homogeneous and filamentous modes, while the plasma jet pattern under negative polarity shows a single ring structure with a homogeneous mode. With respect to the different dielectric materials, the plasma jet interaction with dielectric materials under positive polarity presents different pattern structures with a large number of random filamentous appearing on the outer edge of the pattern. As for the plasma jet pattern under negative polarity, the pattern always shows a uniform pattern without any discharge filaments observed when the plasma jet toughs with different dielectric materials.

Acknowledgments

This work was supported by the National Natural Science Foundation of China (Grant Nos. 51307135, 51307134, 51521065, and 51221005), and the State Key Laboratory of Electrical Insulation and Power Equipment (Grant Nos. EIPE17309 and EIPE 14123).

References

[1] Marshall S E, Jenkins A T A, Al-Bataineh S A, Short R D, Hong S H, Thet N T, Oh J S, Bradley J W and Szili E J 2013 *J. Phys. D: Appl. Phys.* **46** 185401
[2] Kong M G, Kroesen G, Morfill G, Nosenko T, Shimizu T, Van Dijk J and Zimmermann J L 2009 *New J. Phys.* **11** 115012
[3] Jijie R, Pohoata V and Topala I 2012 *Appl. Phys. Lett.* **101** 144103
[4] Norberg S A, Johnsen E and Kushner M J 2015 *Plasma Sources Sci. Technol.* **24** 035026
[5] Xia Y, Liu D P, Wang W C, Bi Z H, Wang X Y, Niu J H, Li L F, Song Y and Qi Z H 2016 *J. Phys. D: Appl. Phys.* **49** 165202
[6] Lu X, Naidis G V, Laroussi M and Ostrikov K 2014 *Phys. Rep.* **540** 123–66
[7] Boeuf J P, Yang L L and Pitchford L C 2013 *J. Phys. D: Appl. Phys.* **46** 015201
[8] Naidis G V 2011 *Appl. Phys. Lett.* **98** 141501
[9] Weatherford B R, Xiong Z M, Barnat E V and Kushner M J 2014 *J. Appl. Phys.* **116** 103305
[10] Hasan M I and Bradly J W 2015 *J. Phys. D: Appl. Phys.* **48** 435201
[11] Wang L J, Zheng Y S and Jia S L 2016 *Phys. Plasmas* **23** 103504
[12] Graves D B 2014 *Plasma Process. Polym.* **11** 1120–7
[13] Breden D and Raja L L 2014 *Plasma Sources Sci. Technol.* **23** 065020
[14] Norberg S A, Johnsen E and Kushner M J 2015 *J. Appl. Phys.* **118** 013301
[15] Guaitella O and Sobota A 2015 *J. Phys. D: Appl. Phys.* **48** 255202
[16] Tian W and Kushner M J 2014 *J. Phys. D: Appl. Phys.* **47** 165201
[17] Norberg S A, Tian W, Johnsen E and Kushner M J 2014 *J. Phys. D: Appl. Phys.* **47** 475203
[18] Zhang C, Shao T, Zhou Y, Fang Z, Yan P and Yang W 2014 *Appl. Phys. Lett.* **105** 044102
[19] Xiong Q, Nikiforov A Y, Lu X P and Leys C J 2010 *J. Phys. D: Appl. Phys.* **43** 415201
[20] Luo S Q, Denning C M and Scharer J E 2008 *J. Appl. Phys.* **104** 013301
[21] Liu Z J, Wang W C, Yang Z D, Zhang S, Yang Y and Tang K 2013 *J. Appl. Phys.* **113** 233305
[22] Wang R X, Zhang K, Shen Y, Zhang C, Zhu W D and Shao T 2016 *Plasma Sources Sci. Technol.* **25** 015020
[23] Kang W S, Hur M and Song Y H 2015 *Appl. Phys. Lett.* **107** 094101
[24] Xiong Z, Lu X P, Xian Y, Jiang Z and Pan Y 2010 *J. Appl. Phys.* **108** 103303
[25] Algwari Q T and Connell D O 2011 *IEEE Trans. Plasma Sci.* **39** 2368–9
[26] Wild R, Gerling T, Bussiahn R, Weltmann K D and Stollenwerk L 2014 *J. Phys. D: Appl. Phys.* **47** 042001